Adaptive numerical solution of thick plates using first-order shear deformation theory. Part I: Error estimates.

M.J. Ludwig[1], Simon Shaw and J.R. Whiteman
Department of Mathematics and Statistics,
Brunel University, Uxbridge, Middlesex, UB8 3PH, U.K.

A posteriori error estimation employing both a residual based estimator and a recovery based estimator is discussed. Interest is focused upon the application to Reissner-Mindlin type thick plates modelled using first-order shear deformation theory, and our investigation limited to uniform meshes of bilinear quadrilateral elements. Numerical results for selected test problems are presented for the resulting error estimators and discussed.

Keywords: A posteriori, error estimate, thick plates, first-order shear deformation.

I. INTRODUCTION

The importance of calculable error estimates for any numerical solution has now been accepted, see for example Oden, Demkowicz, Rachowicz and Westermann, [9]. This paper considers *a posteriori* error estimation for finite element solution of Reissner-Mindlin type thick plates, modelled using first-order shear deformation theory (hereinafter referred to FSDT).

We outline the formulation given by Reddy in [10] below in Section II. and then introduce a standard weak formulation in Section III.. From this the finite element approximation follows in Section IV. where we also take the opportunity of describing a reduced quadrature scheme. In Section V. we derive a residual-based *a posteriori* energy-error estimate using the technique described for linear elasticity by Johnson and Hansbo in [4]. The estimate contains certain interpolation-error constants, which—in general—have to estimated numerically, and in Section VI. we describe a procedure for this.

[1]Ludwig would like to acknowledge the support of a research studentship from the Engineering and Physical Sciences Research Council

An alternative *a postriori* error estimate is derived in Section VII., and is of the ZZ recovery type, as described by Zienkiewicz and Zhu in [13]. The performance of both of these estimators on uniform meshes are compared in Section VIII. using model exact solutions. The residual estimator overestimates the error by orders of magnitude and to address this we compute a *calibration constant* which can be used to "tune" the estimator. We finish with Section IX. where we point towards the adaptive solution strategy, based on quadrilateral transition elements, presented in [6].

II. FIRST-ORDER THEORY FOR LINEAR ELASTIC PLATE DEFORMATION

We consider the small deformation of a Reissner-Mindlin (see [11, 7]) thick plate of thickness t, in plane stress, and modelled using FSDT. This model includes the effects of transverse shear terms by allowing plane sections initially normal to the midplane of the plate to remain planar, but to rotate relative to the midplane during deformation. The plate is thus described in terms of its midplane $(x_1, x_2) \in \Omega \in \mathbb{R}^2$ with boundary $\partial\Omega$ and the x_3-axis normal to the midplane. We assume throughout that Ω is square.

As given in Reddy, [10], the global displacements u_1, u_2 and u_3 of the plate can be described as,

$$\begin{aligned} u_1(x_1, x_2, x_3) &= u(x_1, x_2) + x_3\psi_1(x_1, x_2), \\ u_2(x_1, x_2, x_3) &= v(x_1, x_2) + x_3\psi_2(x_1, x_2), \\ u_3(x_1, x_2, x_3) &= w(x_1, x_2), \end{aligned} \tag{2.1}$$

where u, v and w are the displacements in the x_1, x_2 and x_3-axis directions of the point $(x_1, x_2) \in \Omega$ and ψ_1 and ψ_2 are rotations about the x_2 and x_1 axes at the point $(x_1, x_2) \in \Omega$ respectively. The term first-order in FSDT arises due to the order of approximation of the three global displacements which can be seen above to be power series of the thickness coordinate. The small strains associated with the above displacement field are given in the usual way as ε_{ij} where,

$$\varepsilon_{ij} = \frac{1}{2}\left(\frac{\partial u_i}{\partial x_j} + \frac{\partial u_j}{\partial x_i}\right). \tag{2.2}$$

By using contracted notation, where $\varepsilon_{ii} \equiv \varepsilon_i$ for $i = 1, 2, 3$ and also where $2\varepsilon_{12} \equiv \varepsilon_4$, $2\varepsilon_{13} \equiv \varepsilon_5$ and $2\varepsilon_{23} \equiv \varepsilon_6$ it is possible to use (2.1) with (2.2) to express the strains for the plate problem in the form,

$$\varepsilon_i = \varepsilon_i^{(0)} + x_3\varepsilon_i^{(1)} \quad i = 1, 2, 4, 5, 6. \tag{2.3}$$

Here the superscripts (0) and (1) refer, respectively, to strains induced by the axial displacements u, v and w, and the rotations ψ_1 and ψ_2.

We assume that the plate constitutive relations obey Hooke's law which, for an isotropic linear elastic material in two dimensions, relates the stress tensor $\{\sigma_{ij}\}$ to the strain tensor $\{\varepsilon_{ij}\}$ in the following way,

$$\sigma_{ij}(\mathbf{u}) = \lambda\left\{\sum_{k=1}^{3}\varepsilon_{kk}(\mathbf{u})\right\}\delta_{ij} + 2\mu\varepsilon_{ij}(\mathbf{u}), \quad 1 \le i, j \le 2. \tag{2.4}$$

where the Lamé coefficients λ and μ cast in the plane stress setting may be expressed as,

$$\lambda = \frac{E\nu}{1-\nu^2} \quad \text{and} \quad \mu = \frac{E}{2(1+\nu)}, \tag{2.5}$$

for an isotropic material with Young's modulus E and Poisson's ratio ν.

As described by Reddy, [10], the plate problem equilibrium equations are,

$$\frac{\partial N_1}{\partial x_1} + \frac{\partial N_4}{\partial x_2} = 0, \tag{2.6}$$

$$\frac{\partial N_4}{\partial x_1} + \frac{\partial N_2}{\partial x_2} = 0, \tag{2.7}$$

$$\frac{\partial Q_5}{\partial x_1} + \frac{\partial Q_6}{\partial x_2} + q = 0, \tag{2.8}$$

$$\frac{\partial M_1}{\partial x_1} + \frac{\partial M_4}{\partial x_2} - Q_5 = 0, \tag{2.9}$$

$$\frac{\partial M_4}{\partial x_1} + \frac{\partial M_2}{\partial x_2} - Q_6 = 0, \tag{2.10}$$

where N_i and M_i for $i = 1, 2, 4$ are the stress and bending moment resultants respectively. For a plate of thickness t we have that,

$$\begin{bmatrix} N_1 \\ N_2 \\ N_4 \end{bmatrix} = \begin{bmatrix} A_{11} & A_{12} & A_{14} \\ A_{12} & A_{22} & A_{24} \\ A_{14} & A_{24} & A_{44} \end{bmatrix} \begin{bmatrix} \varepsilon_1^{(0)} \\ \varepsilon_2^{(0)} \\ \varepsilon_4^{(0)} \end{bmatrix} \text{ and } \begin{bmatrix} M_1 \\ M_2 \\ M_4 \end{bmatrix} = \begin{bmatrix} D_{11} & D_{12} & D_{14} \\ D_{12} & D_{22} & D_{24} \\ D_{14} & D_{24} & D_{44} \end{bmatrix} \begin{bmatrix} \varepsilon_1^{(1)} \\ \varepsilon_2^{(1)} \\ \varepsilon_4^{(1)} \end{bmatrix}, \tag{2.11}$$

where Equation (2.3) has been used and where A_{ij} and D_{ij}, for $i, j = 1, 2, 4$, are the in-plane and bending stiffnesses of the plate respectively. These are given by,

$$(A_{ij}, D_{ij}) = \int_{-\frac{t}{2}}^{\frac{t}{2}} C_{ij} \left(1, x_3^2\right) \, dx_3, \quad i, j = 1, 2, 4. \tag{2.12}$$

It should be noted here that in the case of laminated plates the above integration is performed over each laminate and then summed. Such a procedure will also yield bending-stretching stiffnesses as detailed by Ochoa and Reddy, [8] and performed in Ludwig [5]. In Equation (2.12) the terms C_{ij} arise from Hooke's law and, in addition, the transverse shear force resultants have the form,

$$\begin{bmatrix} Q_5 \\ Q_6 \end{bmatrix} = \begin{bmatrix} A_{55} & A_{56} \\ A_{56} & A_{66} \end{bmatrix} \begin{bmatrix} \varepsilon_5^{(0)} \\ \varepsilon_6^{(0)} \end{bmatrix}, \tag{2.13}$$

for,

$$A_{ij} = K_i K_j \int_{-\frac{t}{2}}^{\frac{t}{2}} C_{ij} \, dx_3 \quad i, j = 5, 6, \tag{2.14}$$

and where K_i and K_j are shear correction coefficients which, for FSDT are taken to be $K_i^2 = K_j^2 = 5/6$ as also detailed in [8].

The natural boundary conditions for the FSDT modelled plate have the form,

$$\begin{aligned} N_n = \hat{N}_n, &\quad \text{on} \quad \partial\Omega \setminus \Gamma_1 \equiv \hat{\Gamma}_1, \\ N_s = \hat{N}_s, &\quad \text{on} \quad \partial\Omega \setminus \Gamma_2 \equiv \hat{\Gamma}_2, \\ Q_n = \hat{Q}_n, &\quad \text{on} \quad \partial\Omega \setminus \Gamma_3 \equiv \hat{\Gamma}_3, \\ M_n = \hat{M}_n, &\quad \text{on} \quad \partial\Omega \setminus \Gamma_4 \equiv \hat{\Gamma}_4, \\ M_s = \hat{M}_s, &\quad \text{on} \quad \partial\Omega \setminus \Gamma_5 \equiv \hat{\Gamma}_5, \end{aligned}$$

where Γ_i for $i = 1, 2, 3, 4, 5$ are the portions of the boundary on which u_n, u_s, w, ψ_n and ψ_s are specified respectively. In the above the subscripts n and s denote the normal and tangential components to the boundary whilst $\hat{N}_n$, $\hat{N}_s$, $\hat{Q}_n$, $\hat{M}_n$ and $\hat{M}_s$ are given data derived from the tractions. (For more detail we refer to Reddy [10].)

It is more convenient to express the above boundary conditions in terms of the stress and bending moment resultants introduced earlier in equations (2.6)—(2.10). When this is done we have that,

$$\begin{aligned} \hat{N}_n &= N_1 n_1 + N_4 n_2, \\ \hat{N}_s &= N_4 n_1 + N_2 n_2, \\ \hat{Q}_n &= Q_5 n_1 + Q_6 n_2, \\ \hat{M}_n &= M_1 n_1 + M_4 n_2, \\ \hat{M}_s &= M_4 n_1 + M_2 n_2, \end{aligned} \tag{2.15}$$

on $\hat{\Gamma}_i$ for $i = 1, 2, 3, 4, 5$ respectively. The essential boundary conditions are given by specifying u, v, w, ψ_1 and ψ_2 on boundary portions Γ_i for $i = 1, 2, 3, 4, 5$ respectively.

III. WEAK FORMULATION

The weak formulation of the plate problem is formed by taking the scalar product of Equations (2.6)-(2.10) with a test function vector $\mathbf{v} \in V$ where,

$$V = \left\{ \mathbf{v} \in \left[H^1(\Omega)\right]^5 : \mathbf{v} \text{ satisfies essential b.c. of Section (II.)} \right\}, \tag{3.1}$$

and integrating by parts over Ω. This process trades differentiation from the resultants onto the test functions and yields the task of finding $\mathbf{u} \in V$ such that,

$$a(\mathbf{u}, \mathbf{v}) = F(\mathbf{v}), \quad \forall\ \mathbf{v} \in V, \tag{3.2}$$

where,

$$a(\mathbf{u}, \mathbf{v}) \equiv \int_\Omega \left(\mathbf{B}^b \mathbf{u}\right)^T \mathbf{C}^b \left(\mathbf{B}^b \mathbf{v}\right)\, d\mathbf{x} + \int_\Omega \left(\mathbf{B}^s \mathbf{u}\right)^T \mathbf{C}^s \left(\mathbf{B}^s \mathbf{v}\right)\, d\mathbf{x}, \tag{3.3}$$

and,

$$\begin{aligned} F(\mathbf{v}) \equiv \int_\Omega v_3 q\, d\mathbf{x} \ &+ \int_{\hat{\Gamma}_1} \hat{N}_n v_1\, ds + \int_{\hat{\Gamma}_2} \hat{N}_s v_2\, ds \\ &+ \int_{\hat{\Gamma}_3} \hat{Q}_n v_3\, ds + \int_{\hat{\Gamma}_4} \hat{M}_n v_4\, ds + \int_{\hat{\Gamma}_5} \hat{M}_s v_5\, ds, \end{aligned} \tag{3.4}$$

where $\hat{N}_n$, $\hat{N}_s$, $\hat{Q}_n$, $\hat{M}_n$ and $\hat{M}_s$ are as given in Equation (2.15) and $\mathbf{n} = n_1\mathbf{i} + n_2\mathbf{j}$ is the unit outward normal in each boundary integral to the corresponding boundary edge. In Equation (3.3) the terms $\mathbf{B}^b, \mathbf{B}^s, \mathbf{C}^b$ and $\mathbf{C}^s$ have been introduced. This is due to the fact that there are terms in the formulation which arise from plate bending terms and transverse shear terms denoted respectively by a superscript b and superscript s. The terms $\mathbf{B}^b$ and $\mathbf{B}^s$ are differential operators acting on $\mathbf{u}$ and $\mathbf{v}$ so that, for example,

$$\mathbf{B}^b\mathbf{v} = \left[\frac{\partial v_1}{\partial x_1}, \frac{\partial v_2}{\partial x_2}, \frac{\partial v_1}{\partial x_2} + \frac{\partial v_2}{\partial x_1}, \frac{\partial v_4}{\partial x_1}, \frac{\partial v_5}{\partial x_2}, \frac{\partial v_4}{\partial x_2} + \frac{\partial v_5}{\partial x_2}\right]^T, \tag{3.5}$$

and,

$$\mathbf{B}^s\mathbf{v} = \left[\frac{\partial v_3}{\partial x_1} + v_4, \frac{\partial v_3}{\partial x_2} + v_5\right]^T. \tag{3.6}$$

The terms $\mathbf{C}^b$ and $\mathbf{C}^s$ are matrices which depend upon the material properties involved and arise from the definitions of the force and moment resultants and the definitions of the transverse shear forces given previously. The matrices have the forms,

$$\mathbf{C}^b = \begin{bmatrix} A_{11} & A_{12} & A_{14} & 0 & 0 & 0 \\ A_{12} & A_{22} & A_{24} & 0 & 0 & 0 \\ A_{14} & A_{24} & A_{44} & 0 & 0 & 0 \\ 0 & 0 & 0 & D_{11} & D_{12} & D_{14} \\ 0 & 0 & 0 & D_{12} & D_{22} & D_{24} \\ 0 & 0 & 0 & D_{14} & D_{24} & D_{44} \end{bmatrix}, \quad \mathbf{C}^s = \begin{bmatrix} A_{55} & A_{56} \\ A_{56} & A_{66} \end{bmatrix}, \tag{3.7}$$

where A_{ij} and D_{ij} for $i, j = 1, 2, 4$ are as defined in Equation (2.12) and A_{ij} for $i, j = 5, 6$ are as defined in Equation (2.14). It should be noted again that for a laminated plate additional elements of $\mathbf{C}^b$ may well be non-zero, this is considered by Ludwig in [5].

IV. PLATE FINITE ELEMENT MODEL

Consider the finite element subdivision Υ_h of Ω into non-overlapping elements Ω_k of size $h = h_k$. In addition, for each element $\Omega_k \in \Upsilon_h$ let there exist a positive integer p_k and also let $P_{p_k}(\Omega_k)$ be a space of polynomials on Ω_k containing the set of polynomials over Ω_k of degree at most p_k then the finite element space is given as,

$$V^h = \left\{\mathbf{v}_h \in V : \mathbf{v}_h \text{ is continuous on } \Omega, \mathbf{v}_h|_{\Omega_k} \in [P_{p_k}(\Omega_k)]^5 \ \forall\ \Omega_k \in \Upsilon_h\right\}. \tag{4.1}$$

The Galerkin finite element method is applied to Equation (3.2) so that a solution $\mathbf{u}_h \in V^h \subset V$ is sought such that,

$$a(\mathbf{u}_h, \mathbf{v}_h) = F(\mathbf{v}_h) \quad \forall \quad \mathbf{v}_h \in V^h. \tag{4.2}$$

Since the force and moment resultants contain, at most, only the first derivatives of the dependent variables u, v, w, ψ_1 and ψ_2, all may be approximated using Lagrange interpolation functions. This means that the plate bending element of the first-order plate theory may be a C^0 element and thus each of the displacements u, v, w, ψ_1 and ψ_2 are approximated over each element as,

$$\alpha(x_1, x_2) \approx \alpha_h(\mathbf{x}) := \sum_{j=1}^{n} \alpha_j^h \phi_j(\mathbf{x}), \qquad \text{for } \alpha = u, v, w, \psi_1 \text{ or } \psi_2, \tag{4.3}$$

where n is the number of nodes per element, α_j^h denotes the value of $\alpha = u, v, w, \psi_1$ or ψ_2 at node j and $\phi_j(\mathbf{x})$ are element shape functions of Lagrange type. The finite element model is then obtained by substituting expressions (4.3) for u, v, w, ψ_1 and ψ_2 into Equation (4.2), and then taking $\mathbf{v}$ equal to each basis function in turn. The element stiffness matrix for a typical element Ω_k may then be expressed as,

$$\mathbf{K}_k = (K_{ij})_{i,j=1}^{5n},$$

where each K_{ij} is given by,

$$K_{ij} = a(\boldsymbol{\phi}_i, \boldsymbol{\phi}_j)|_{\Omega_k} = \int_{\Omega_k} \left(\mathbf{B}^b \boldsymbol{\phi}_i\right)^T \mathbf{C}^b \left(\mathbf{B}^b \boldsymbol{\phi}_j\right)\, d\mathbf{x} + \int_{\Omega_k} \left(\mathbf{B}^s \boldsymbol{\phi}_i\right)^T \mathbf{C}^s \left(\mathbf{B}^s \boldsymbol{\phi}_j\right)\, d\mathbf{x},$$

for $i, j = 1, \ldots, 5n$ and where the vectors $\boldsymbol{\phi}_i$ for $i = 1, \ldots, 5n$ are as follows,

$$\left.\begin{array}{ll} \boldsymbol{\phi}_{5m-4} & = [\phi_m, 0, 0, 0, 0]^T \\ \boldsymbol{\phi}_{5m-3} & = [0, \phi_m, 0, 0, 0]^T \\ \boldsymbol{\phi}_{5m-2} & = [0, 0, \phi_m, 0, 0]^T \\ \boldsymbol{\phi}_{5m-1} & = [0, 0, 0, \phi_m, 0]^T \\ \boldsymbol{\phi}_{5m} & = [0, 0, 0, 0, \phi_m]^T \end{array}\right\} \quad \text{for } m = 1, \ldots, n.$$

The Lagrange type elements used in this work have a weakness that they become stiff when used to model thin plates. This behaviour is called locking which is undesirable in that it causes an underprediction of displacements and the plate appears stiffer than the material properties would suggest. Although thin plates are not of concern in this work the point at which a plate becomes classed as thin is not clearly defined. Consequently the following discussion details briefly a numerical technique employed to eradicate locking.

As observed by Averill and Reddy, [1], locking is caused by a state of zero transverse shearing strain being imposed on the model in the thin plate scenario. Shear deformable finite elements are unable to model this state and the phenomenon known as shear locking is created.

In order to combat the effect of locking, a reduced integration scheme can be used. For the bilinear element numerical integration would ordinarily be carried out using a 2×2 Gauss quadrature scheme and this is indeed the case for plates. The exception, however, is that a single point or 1×1 Gauss quadrature scheme is employed to integrate the transverse shear terms in the element stiffness matrices. In this way a bilinear element which uses reduced integration to integrate the transverse shear strain terms in the element stiffness matrix should also accurately model thin plate behaviour. This is termed *selective* integration.

TABLE I. Counts of zero eigenvalues for element stiffness matrix $\mathbf{K}_k$.

Integration Scheme		Number of zero eigenvalues		
Bending Terms	Shear Terms	$\mathbf{K}_k^b$	$\mathbf{K}_k^s$	$\mathbf{K}_k = \mathbf{K}_k^b + \mathbf{K}_k^s$
exact	exact	7	4	3
2×2	2×2	7	4	3
2×2	1×1	7	10	5
1×1	1×1	9	10	7

Table (I) shows the effect upon the computed element stiffness matrix upon varying the quadrature used. It can be seen that changing the integration scheme produces a subsequent change in the number of zero eigenvalues of the element stiffness matrix. It is important to note that shear locking does not involve membrane deformation and so in-plane displacements u and v are assumed to be zero. Following such an assumption the element stiffness matrix will have three zero eigenvalues. These correspond to the three rigid body motions which are a transverse displacement and two rotations, each of which can be taken to rotate around the x_1 or x_2 coordinate axes. From Table (I) it can be seen that by using selective integration the element stiffness matrix $\mathbf{K}_k$ will have five zero eigenvalues (these results have been obtained with Mathematica, [12]). Thus the reduced integration has introduced two extra zero eigenvalues. As previously mentioned, it is required that the product of the shear stiffness matrix and the displacement vector be zero as the span-to-thickness ratio tends to infinity. The use of reduced integration enables this by making the shear stiffness matrix singular. In such a situation a non-trivial displacement may be obtained since the product of the non-trivial displacement and the singular matrix can be zero.

V. JOHNSON-HANSBO TYPE ERROR ESTIMATE FOR PLATES (JH-P)

In this section we shall build on the Johnson-Hansbo estimation technique described in [4] for linear elasticity and produce a new energy norm error estimator for the plate model described by Equations (2.6)-(2.10).

Since Equation (3.2) holds for all $\mathbf{v} \in V$ it must also hold for $\mathbf{v}_h \in V^h \subset V$. It is thus possible to subtract Equation (4.2) from the restricted form of Equation (3.2) to give the orthogonality condition,

$$a(\mathbf{u} - \mathbf{u}_h, \mathbf{v}_h) = 0 \quad \forall\ \mathbf{v}_h \in V^h. \tag{5.1}$$

Let the finite element error be,

$$\mathbf{e} = \mathbf{u} - \mathbf{u}_h,$$

and define the energy norm of $\mathbf{e}$ over the problem domain Ω as,

$$\|\mathbf{e}\|^2_{E(\Omega)} = a(\mathbf{e}, \mathbf{e}) = a(\mathbf{u} - \mathbf{u}_h, \mathbf{e}) = a(\mathbf{u} - \mathbf{u}_h, \mathbf{e} - \pi_h \mathbf{e}), \tag{5.2}$$

using the orthogonality condition of Equation (5.1) with $\mathbf{v}_h = \pi_h \mathbf{e} \in V_h$ and where π_h is an interpolation operator $\pi_h : \left[H^1(\Omega)\right]^5 \to V^h$. Thus,

$$\|\mathbf{e}\|^2_{E(\Omega)} = a(\mathbf{u}, \mathbf{e} - \pi_h \mathbf{e}) - a(\mathbf{u}_h, \mathbf{e} - \pi_h \mathbf{e}),$$

which, by using Equation (3.2) with $\mathbf{v} = \mathbf{e} - \pi_h \mathbf{e} \in V$ enables the error to be finally written as,

$$\|\mathbf{e}\|^2_{E(\Omega)} = F(\mathbf{e} - \pi_h \mathbf{e}) - a(\mathbf{u}_h, \mathbf{e} - \pi_h \mathbf{e}). \tag{5.3}$$

In order to proceed it will be necessary to integrate the bilinear form by parts over each element in order to trade the differentiation from the interpolation error terms in Equation (5.3). This enables the error to be expressed as,

$$\|\mathbf{e}\|^2_{E(\Omega)} = \sum_{k=1}^{N} \int_{\Omega_k} (\mathbf{f} + \operatorname{div} \mathbf{T}(\mathbf{u}_h) - \mathbf{q}(\mathbf{u}_h)) \cdot (\mathbf{e} - \pi_h \mathbf{e})\, d\mathbf{x}$$

$$
\begin{aligned}
&-\sum_{k=1}^{N}\int_{\partial\Omega_k}(\mathbf{T}(\mathbf{u}_h)\,\mathbf{n}_k)\cdot(\mathbf{e}-\pi_h\mathbf{e})\,ds\\
&+\int_{\hat{\Gamma}_1}\hat{N}_n(e_1-\pi_h e_1)\,ds+\int_{\hat{\Gamma}_2}\hat{N}_s(e_2-\pi_h e_2)\,ds+\int_{\hat{\Gamma}_3}\hat{Q}_n(e_3-\pi_h e_3)\,ds\\
&+\int_{\hat{\Gamma}_4}\hat{M}_n(e_4-\pi_h e_4)\,ds+\int_{\hat{\Gamma}_5}\hat{M}_s(e_5-\pi_h e_5)\,ds, \qquad (5.4)
\end{aligned}
$$

where $\mathbf{f}=(0,0,q,0,0)^T$ is the applied transverse load, $\mathbf{n}_k$ is the unit outward normal to the boundary $\partial\Omega_k$ of element Ω_k and, for the integrals over boundary portions $\hat{\Gamma}_i$ for $i=1,2,3,4,5$ of $\partial\Omega$, the interpolation error vector has been separated into component form. In the above $\mathbf{T}(\mathbf{u}_h)$ and $\mathbf{q}(\mathbf{u}_h)$ are of the form,

$$
\mathbf{T}(\mathbf{u}_h)\equiv\mathbf{T}=\begin{bmatrix}T_{11} & T_{12}\\ T_{21} & T_{22}\\ T_{31} & T_{32}\\ T_{41} & T_{42}\\ T_{51} & T_{52}\end{bmatrix}\equiv\begin{bmatrix}N_1^h & N_4^h\\ N_4^h & N_2^h\\ Q_5^h & Q_6^h\\ M_1^h & M_4^h\\ M_4^h & M_2^h\end{bmatrix}\quad\text{and}\quad\mathbf{q}(\mathbf{u}_h)\equiv\mathbf{q}=\begin{bmatrix}0\\0\\0\\Q_5^h\\Q_6^h\end{bmatrix} \qquad (5.5)
$$

where we define,

$$
\operatorname{div}\mathbf{T}:=\left(\sum_{j=1}^{2}\frac{\partial T_{ij}}{\partial x_j}\right)_{i=1}^{5}\quad\text{and}\quad\mathbf{T}\,\mathbf{n}_k:=\left(\sum_{j=1}^{2}T_{ij}n_j\right)_{i=1}^{5},
$$

and where $\mathbf{u}_h$ is contained in the terms N_i^h, M_i^h for $i=1,2,4$ and Q_i^h for $i=5,6$ given by Equations (2.11) and (2.13) (the superscript h has been used to signify the presence of the finite element solution). The left side of the integrand for the element boundary integral thus has the form,

$$
\mathbf{T}(\mathbf{u}_h)\,\mathbf{n}_k=\begin{bmatrix}N_1^h & N_4^h\\ M_4^h & N_2^h\\ Q_5^h & Q_6^h\\ M_1^h & M_4^h\\ M_4^h & M_2^h\end{bmatrix}\begin{bmatrix}n_1\\ n_2\end{bmatrix}, \qquad (5.6)
$$

for the interior element edges of element Ω_k. For edges of element Ω_k which coincide with the boundary portions $\hat{\Gamma}_i$ for $i=1,2,3,4,5$ we have,

$$
\mathbf{T}(\mathbf{u}_h)\,\mathbf{n}_k=\left[\,N_n^h\ N_s^h\ Q_n^h\ M_n^h\ M_s^h\,\right]^T, \qquad (5.7)
$$

the terms of which are defined as in Equation (2.15) but again noting the presence now of the finite element solution. Denoting S to be the set of all internal element edges it is clear that upon integrating around the perimeter of each element we are integrating along element edges $s\in S$ which lie in the open set Ω as well as those edges which lie on $\partial\Omega$ and thus not in set S. Further, in performing the integration over all elements, it is clear that the integration will be performed twice along all such internal element edges $s\in S$. As described in [4] this introduces the notion of a 'jump' across a typical edge s which shall henceforth be denoted by $[\mathbf{T}(\mathbf{u}_h)\,\mathbf{n}_s]$ and where $\mathbf{n}_s$ can be considered as the unit normal to the edge s. The definition of the stress jump $[\mathbf{T}(\mathbf{u}_h)\,\mathbf{n}_s]$ can be thought of as taking the difference of the quantity defined in Equation (5.6) as we approach the edge from both sides. We thus have, for a point $\mathbf{x}$ on internal edge $s \in S$,

$$[\mathbf{T}(\mathbf{u}_h)\,\mathbf{n}_s](\mathbf{x}) := \lim_{t\to 0^+} \mathbf{T}(\mathbf{u}_h(\mathbf{x}+t\mathbf{n}_s))\,\mathbf{n}_s(\mathbf{x}) - \lim_{t\to 0^+} \mathbf{T}(\mathbf{u}_h(\mathbf{x}-t\mathbf{n}_s))\,\mathbf{n}_s(\mathbf{x}). \quad (5.8)$$

It is thus possible to express Equation (5.4) as,

$$\|\mathbf{e}\|^2_{E(\Omega)} = E_1 + E_2 \le |E_1| + |E_2|, \quad (5.9)$$

where,

$$E_1 = \sum_{k=1}^{N} \int_{\Omega_k} \mathcal{R}_1(\mathbf{u}_h)\cdot(\mathbf{e}-\pi_h\mathbf{e})\,d\mathbf{x}, \quad (5.10)$$

$$E_2 = \sum_{k=1}^{N} \int_{\partial\Omega_k} h_k\mathcal{R}_2(\mathbf{u}_h)\cdot(\mathbf{e}-\pi_h\mathbf{e})\,ds, \quad (5.11)$$

with,

$$\mathcal{R}_1(\mathbf{u}_h) = \mathbf{f} + \operatorname{div}\mathbf{T}(\mathbf{u}_h) - \mathbf{q}(\mathbf{u}_h), \qquad \text{on } \Omega_k, \quad (5.12)$$

and,

$$\mathcal{R}_2(\mathbf{u}_h) = \begin{cases} \dfrac{1}{2h_k}\left[\mathbf{T}(\mathbf{u}_h)\mathbf{n}_s\right], & \text{on } s\subset\partial\Omega_k \text{ if } s\in S,\\ \dfrac{1}{h_k}\left[\hat{N}_n - N_n^h, 0,0,0,0\right]^T, & \text{on } \partial\Omega_k\cap\hat{\Gamma}_1,\\ \dfrac{1}{h_k}\left[0,\hat{N}_s - N_s^h, 0,0,0\right]^T, & \text{on } \partial\Omega_k\cap\hat{\Gamma}_2,\\ \dfrac{1}{h_k}\left[0,0,\hat{Q}_n - Q_n^h, 0,0\right]^T, & \text{on } \partial\Omega_k\cap\hat{\Gamma}_3,\\ \dfrac{1}{h_k}\left[0,0,0,\hat{M}_n - M_n^h, 0\right]^T, & \text{on } \partial\Omega_k\cap\hat{\Gamma}_4,\\ \dfrac{1}{h_k}\left[0,0,0,0,\hat{M}_s - M_s^h\right]^T, & \text{on } \partial\Omega_k\cap\hat{\Gamma}_5, \end{cases} \quad (5.13)$$

where $\mathbf{q}(\mathbf{u}_h) = \left[0,0,0,Q_5^h,Q_6^h\right]^T$. In [4] upper bounds are given for the interpolation error $\mathbf{e}-\pi_h\mathbf{e}$ measured in L_2-norms. These bounds are of use in determining the final error estimator and, as described by Ludwig in [5], take the form,

$$\|\mathbf{e}-\pi_h\mathbf{e}\|_{L_2(\Omega_k)} \le C^i_{1,k} h_k \|\mathbf{e}\|_{E(\Omega_k)}, \quad (5.14)$$

and,

$$\|\mathbf{e}-\pi_h\mathbf{e}\|_{L_2(\partial\Omega_k)} \le C^i_{2,k} h_k^{\frac{1}{2}} \|\mathbf{e}\|_{E(\Omega_k)}, \quad (5.15)$$

where,

$$C^i_{1,k} = \sup_{\boldsymbol{\tau}\in V_\epsilon} \frac{h_k^{-1}\|\boldsymbol{\tau}-\pi_h\boldsymbol{\tau}\|_{L_2(\Omega_k)}}{\|\boldsymbol{\tau}\|_{E(\Omega_k)}}, \quad (5.16)$$

and,

$$C^i_{2,k} = \sup_{\boldsymbol{\tau}\in V_\epsilon} \frac{h_k^{-\frac{1}{2}}\|\boldsymbol{\tau}-\pi_h\boldsymbol{\tau}\|_{L_2(\partial\Omega_k)}}{\|\boldsymbol{\tau}\|_{E(\Omega_k)}}, \quad (5.17)$$

and where $V_\epsilon = \left[H^{1+\epsilon}(\Omega_k)\right]^5$. (This is for any $\epsilon > 0$, since then a nodal interpolant can be defined.) By using the Cauchy-Schwarz inequality and Equations (5.14) and (5.15) on the terms in Equation (5.9) the error may be expressed as,

$$\|\mathbf{e}\|_{E(\Omega)} \le \left(\sum_k \left[C^i_{1,k} h_k \|\mathcal{R}_1(\mathbf{u}_h)\|_{L_2(\Omega_k)}\right]^2\right)^{\frac{1}{2}} + \left(\sum_k \left[C^i_{2,k} h_k^{\frac{1}{2}} \|h_k \mathcal{R}_2(\mathbf{u}_h)\|_{L_2(\partial\Omega_k)}\right]^2\right)^{\frac{1}{2}}, \tag{5.18}$$

where it is possible to evaluate the right-hand side. It can be seen that this error measure relies upon the computation of the interpolation error constants which will be detailed in the next section. We henceforth refer to the inequality (5.18) as the JH-P estimator.

VI. INTERPOLATION ERROR CONSTANT CALCULATION

To implement the JH-P error estimator we need to specify the interpolation error constants given by Equations (5.16) and (5.17). In this section we outline a method for the numerical approximation of these constants.

Considering the transformation of the general square element Ω_k of side length h_k to the standard unit square element $\hat{\Omega}$ it follows that,

$$a(\mathbf{u},\mathbf{v})|_{\Omega_k} \equiv \frac{1}{h_k^2}\int_{\hat{\Omega}} \left(\hat{\mathbf{B}}^b\hat{\mathbf{u}}\right)^T \mathbf{C}^b \left(\hat{\mathbf{B}}^b\hat{\mathbf{v}}\right) |\mathbf{J}|\, d\hat{\mathbf{x}} + \frac{1}{h_k^2}\int_{\hat{\Omega}} \left(\hat{\mathbf{B}}^s\hat{\mathbf{u}}\right)^T \mathbf{C}^s \left(\hat{\mathbf{B}}^s\hat{\mathbf{v}}\right) |\mathbf{J}|\, d\hat{\mathbf{x}},$$

where $|\mathbf{J}| = h_k^2$, $\mathbf{B}^b = h_k^{-1}\hat{\mathbf{B}}^b$ and $\mathbf{B}^s = h_k^{-1}\hat{\mathbf{B}}^s$. Although substitution of $|\mathbf{J}|$ into the above removes the immediate presence of h_k in the expression, inspection of $\hat{\mathbf{B}}^s$ reveals further terms involving h_k. Taking $\hat{\mathbf{u}} = [\hat{u}_1, \hat{u}_2, \hat{u}_3, \hat{u}_4, \hat{u}_5]^T$ it can be seen that,

$$\hat{\mathbf{B}}^s\hat{\mathbf{u}} = \begin{bmatrix} 0 & 0 & \frac{\partial}{\partial\xi} & h_k & 0 \\ 0 & 0 & \frac{\partial}{\partial\eta} & 0 & h_k \end{bmatrix} \begin{bmatrix} \hat{u}_1 \\ \hat{u}_2 \\ \hat{u}_3 \\ \hat{u}_4 \\ \hat{u}_5 \end{bmatrix} = \begin{bmatrix} \frac{\partial\hat{u}_3}{\partial\xi} + h_k\hat{u}_4 \\ \frac{\partial\hat{u}_3}{\partial\eta} + h_k\hat{u}_5 \end{bmatrix}. \tag{6.1}$$

Thus the contribution of the integrand, $\mathcal{I}$, to the energy norm, using Equation (3.7) may be expressed as,

$$\mathcal{I} = A_{55}\left(\frac{\partial\hat{u}_3}{\partial\xi} + h_k\hat{u}_4\right)^2 + 2A_{56}\left(\frac{\partial\hat{u}_3}{\partial\xi} + h_k\hat{u}_4\right)\left(\frac{\partial\hat{u}_3}{\partial\eta} + h_k\hat{u}_5\right) + A_{66}\left(\frac{\partial\hat{u}_3}{\partial\eta} + h_k\hat{u}_5\right)^2.$$

The interpolation error constants are to be used in adapted meshes with varying values of h_k and ideally we would like them to be independent of h_k. As illustrated above it is not possible to obtain such a formulation in this case. It is thus proposed that the terms involving h_k in the above expression for $\mathcal{I}$ be set to zero in order to provide constants accurate for the limiting case as $h_k \to 0$. Denoting the resulting contribution by $\mathcal{I}^*$ we thus have that,

$$\mathcal{I}^* = A_{55}\left(\frac{\partial\hat{u}_3}{\partial\xi}\right)^2 + 2A_{56}\left(\frac{\partial\hat{u}_3}{\partial\xi}\right)\left(\frac{\partial\hat{u}_3}{\partial\eta}\right) + A_{66}\left(\frac{\partial\hat{u}_3}{\partial\eta}\right)^2.$$

This operation is equivalent to setting the h_k terms in $\hat{\mathbf{B}}^s$ to zero in Equation (6.1). In doing so we obtain $\hat{\mathbf{B}}^*$ which, when used in the bilinear form in place of $\hat{\mathbf{B}}^s$ yields the modified bilinear form $a^*(\mathbf{u},\mathbf{v})$, defined as,

$$a^*(\mathbf{u},\mathbf{v})|_{\hat{\Omega}} := \int_{\hat{\Omega}} \left(\hat{\mathbf{B}}^b\hat{\mathbf{u}}\right)^T \mathbf{C}^b \left(\hat{\mathbf{B}}^b\hat{\mathbf{v}}\right) d\hat{\mathbf{x}} + \int_{\hat{\Omega}} \left(\hat{\mathbf{B}}^*\hat{\mathbf{u}}\right)^T \mathbf{C}^s \left(\hat{\mathbf{B}}^*\hat{\mathbf{v}}\right) d\hat{\mathbf{x}}.$$

Thus we obtain, for the mapped interpolation error constant quotient,

$$(C_1^i)^2 = \sup_{\hat{\mathbf{u}}\in\hat{V}} \frac{\displaystyle\int_{\hat{\Omega}} |\hat{\mathbf{u}} - \pi\hat{\mathbf{u}}|^2 \, d\hat{\mathbf{x}}}{\displaystyle\int_{\hat{\Omega}} \left(\hat{\mathbf{B}}^b\hat{\mathbf{u}}\right)^T \mathbf{C}^b \left(\hat{\mathbf{B}}^b\hat{\mathbf{u}}\right) d\hat{\mathbf{x}} + \int_{\hat{\Omega}} \left(\hat{\mathbf{B}}^*\hat{\mathbf{u}}\right)^T \mathbf{C}^s \left(\hat{\mathbf{B}}^*\hat{\mathbf{u}}\right) d\hat{\mathbf{x}}},$$

where $\hat{V} := [H^{1+\epsilon}(\hat{\Omega})]^5$, for some $\epsilon \in (0,1)$ depending upon the regularity of $\hat{\mathbf{u}}$ (see e.g. [5, Appendix E]).

The interpolation error constant is now independent of h_k and correct for the limiting case as $h_k \to 0$. Thus, denoting the resulting energy norm arising from the modified bilinear form as $\|\cdot\|_{E^*(\hat{\Omega})}$ we may express,

$$(C_1^i)^2 = \sup_{\hat{\mathbf{u}}\in\hat{V}} \frac{\|\hat{\mathbf{u}} - \pi\hat{\mathbf{u}}\|^2_{L_2(\hat{\Omega})}}{\|\hat{\mathbf{u}}\|^2_{E^*(\hat{\Omega})}} \quad \text{and} \quad (C_2^i)^2 = \sup_{\hat{\mathbf{u}}\in\hat{V}} \frac{\|\hat{\mathbf{u}} - \pi\hat{\mathbf{u}}\|^2_{L_2(\partial\hat{\Omega})}}{\|\hat{\mathbf{u}}\|^2_{E^*(\hat{\Omega})}}.$$

For the numerators of the above expressions we are thus concerned with interpolating the vector-valued function $\mathbf{u}$ by $\pi\mathbf{u}$ where, using appropriate shape functions, we may express $\mathbf{u}(\mathbf{x})$ at any point $\mathbf{x}$ in the element as,

$$\mathbf{u}(\mathbf{x}) = \sum_{i=1}^{n} \mathbf{u}(\mathbf{x}_i)\phi_i(\mathbf{x}) = \sum_{i=1}^{n} \mathbf{u}_i\phi_i(\mathbf{x}),$$

where $\mathbf{u}_i$ is the displacement vector evaluated at the nodes $i = 1,\ldots,n$ and $\{\phi_i(\mathbf{x})\}_{i=1}^n$ are the appropriate element shape functions. The interpolant $\pi\mathbf{u}$ evaluated also at any point $\mathbf{x}$ in the element can be similarly expressed as,

$$\pi\mathbf{u}(\mathbf{x}) = \sum_{i=1}^{m} \pi\mathbf{u}(\mathbf{x}_i)\vartheta_i(\mathbf{x}) = \sum_{i=1}^{m} \pi\mathbf{u}_i\vartheta_i(\mathbf{x}),$$

where now $\{\vartheta_i(\mathbf{x})\}_{i=1}^m$ are the shape functions defined over the element and used to describe $\pi\mathbf{u}$. It is recommended by Johnson and Hansbo in [4] that if $P_p(\Omega_k)$ denotes the space of polymonials on element Ω_k of degree at most p, the above supremum values may be approximated by taking sup over the space of polynomials of degree $p+1$. In this way $\{\phi_i(\mathbf{x})\}_{i=1}^9$ will be the standard biquadratic shape functions and the interpolant will be described by bilinear shape functions $\{\vartheta_i(\mathbf{x})\}_{i=1}^4$. By setting $\vartheta_i(\mathbf{x}) = 0$ for $m < i \le n$ it is possible to express the interpolation error as,

$$\mathbf{u}(\mathbf{x}) - \pi\mathbf{u}(\mathbf{x}) = \sum_{i=1}^{n} \mathbf{u}_i\phi_i(\mathbf{x}) - \sum_{i=1}^{m} \pi\mathbf{u}_i\vartheta_i(\mathbf{x}) = \sum_{i=1}^{n} \mathbf{u}_i \left(\phi_i(\mathbf{x}) - \vartheta_i(\mathbf{x})\right),$$

since, at the nodes, $u_i = \pi u_i$ for $i = 1,\ldots,m$. Thus the interpolation error squared may be expressed as,

$$|\mathbf{u}(\mathbf{x}) - \pi\mathbf{u}(\mathbf{x})|^2 = \mathbf{u}^T\mathbf{\Phi}(\mathbf{x})\,\mathbf{u},$$

where $\mathbf{u}$ is the element displacement vector and can be expressed in terms of the nodal displacement vectors $\mathbf{u}_i$ for $i = 1, \ldots, n$ as,

$$\mathbf{u}^T = \left[\mathbf{u}_1^T, \mathbf{u}_2^T, \ldots, \mathbf{u}_n^T\right],$$

and the matrix $\mathbf{\Phi}(\mathbf{x})$ has the form,

$$\mathbf{\Phi}(\mathbf{x}) = \left(\Phi_{ij}(\mathbf{x})\mathbf{I}_5\right)_{i,j=1}^n, \tag{6.2}$$

where,

$$\Phi_{ij}(\mathbf{x}) = \left(\phi_i(\mathbf{x}) - \vartheta_i(\mathbf{x})\right)\left(\phi_j(\mathbf{x}) - \vartheta_j(\mathbf{x})\right) \text{ for } i, j = 1, \ldots, n,$$

and where $\mathbf{I}_5$ is the 5×5 identity matrix. The integration of the terms of $\mathbf{\Phi}(\mathbf{x})$ yield matrix $\mathbf{F} = \left(F_{ij}\mathbf{I}_5\right)_{i,j=1}^n$ where, for the interior interpolation error constant C_1^i,

$$F_{ij} = \int_{\hat{\Omega}} \Phi_{ij}(\mathbf{x})\, d\mathbf{x} \text{ for } i, j = 1, \ldots, n,$$

whilst for the boundary interpolation error constant, C_2^i,

$$F_{ij} = \int_{\partial\hat{\Omega}} \Phi_{ij}(\mathbf{x})\, d\Gamma \text{ for } i, j = 1, \ldots, n.$$

The task of finding the interpolation error constants may thus be expressed as,

$$C_j^i = \sup_{\mathbf{u}\in\mathbb{R}^{5n}} \frac{\mathbf{u}\cdot\mathbf{F}\,\mathbf{u}}{\mathbf{u}\cdot\mathbf{E}\,\mathbf{u}}, \text{ for } j = 1 \text{ or } 2,$$

where $\mathbf{F}$ is as described above and where $\mathbf{E}$ is the element stiffness matrix arising from the modified bilinear form and which may be expressed as,

$$\mathbf{E} = \left(E_{ij}\right)_{i,j=1}^{5n} \text{ with } E_{ij} = \int_{\hat{\Omega}} \left(\mathbf{B}^b\boldsymbol{\phi}_i\right)^T \mathbf{C}^b \left(\mathbf{B}^b\boldsymbol{\phi}_j\right)\, d\mathbf{x} + \int_{\hat{\Omega}} \left(\mathbf{B}^*\boldsymbol{\phi}_i\right)^T \mathbf{C}^s \left(\mathbf{B}^*\boldsymbol{\phi}_j\right)\, d\mathbf{x},$$

for $i, j = 1, \ldots, 5n$ where,

$$\left.\begin{aligned} \boldsymbol{\phi}_{lk-4} &= \left[\phi_l, 0, 0, 0, 0\right]^T \\ \boldsymbol{\phi}_{lk-3} &= \left[0, \phi_l, 0, 0, 0\right]^T \\ \boldsymbol{\phi}_{lk-2} &= \left[0, 0, \phi_l, 0, 0\right]^T \\ \boldsymbol{\phi}_{lk-1} &= \left[0, 0, 0, \phi_l, 0\right]^T \\ \boldsymbol{\phi}_{lk} &= \left[0, 0, 0, 0, \phi_l\right]^T \end{aligned}\right\} \quad \text{for } l = 1, \ldots, n,$$

and where the bilinear form has been modified slightly via the operator $\hat{\mathbf{B}}^*$ to give a value of C_j^i for $j = 1, 2$ independent of element size h_k.

The above supremum value corresponds to the maximum eigenvalue $\lambda_{\max}$ of the generalised eigenvalue problem,

$$\lambda\mathbf{E}\mathbf{u} = \mathbf{F}\mathbf{u},$$

solvable via the use of the QZ algorithm as described by Datta, [3]. Such a technique will be applied in this work in order to obtain the required interpolation error constant values for use in Section (VIII.).

VII. ZIENKIEWICZ-ZHU TYPE ERROR ESTIMATE FOR PLATES (ZZ-P)

In contrast to the error estimation technique illustrated above we shall now apply the Zienkiewicz-Zhu estimator described in [14, 15] to the plate model described in Section (II.). From Section (III.) the weak formulation for the current plate problem yields bilinear form as given by Equation (3.3). From this it is clear that the bending and transverse shear strains may be expressed as,

$$\varepsilon^b(\mathbf{u}) = \mathbf{B}^b\mathbf{u} \quad \text{and} \quad \varepsilon^s(\mathbf{u}) = \mathbf{B}^s\mathbf{u}.$$

Consequently these give rise to stresses $\boldsymbol{\sigma}^b$ and $\boldsymbol{\sigma}^s$ expressed by multiplying with material matrices $\mathbf{C}^b$ and $\mathbf{C}^s$ to give,

$$\boldsymbol{\sigma}^b(\mathbf{u}) = \mathbf{C}^b\varepsilon^b(\mathbf{u}) \quad \text{and} \quad \boldsymbol{\sigma}^s(\mathbf{u}) = \mathbf{C}^s\varepsilon^s(\mathbf{u}).$$

Thus the error of the gradients (stresses) can be expressed as,

$$\mathbf{e}_{\sigma^b} = \boldsymbol{\sigma}^b - \boldsymbol{\sigma}^b_h \quad \text{and} \quad \mathbf{e}_{\sigma^s} = \boldsymbol{\sigma}^s - \boldsymbol{\sigma}^s_h. \tag{7.1}$$

The $\mathbf{u}$, $\boldsymbol{\sigma}^b$ and $\boldsymbol{\sigma}^s$ will generally not be known. Thus substitution of the values $\mathbf{e}_{\sigma^b}$ and $\mathbf{e}_{\sigma^s}$ in Equation (7.1) is made by an approximation to each. The quantities $\boldsymbol{\sigma}^b$ and $\boldsymbol{\sigma}^s$ are replaced with $\boldsymbol{\sigma}^{*b}_h$ and $\boldsymbol{\sigma}^{*s}_h$ respectively which are recovered or post-processed values of $\boldsymbol{\sigma}^b_h$ and $\boldsymbol{\sigma}^s_h$ and which are interpolated between their nodal values by the finite element displacement basis functions. We thus have that,

$$\mathbf{e}_{\sigma^b} \approx \mathbf{e}^*_{\sigma^b} = \boldsymbol{\sigma}^{*b}_h - \boldsymbol{\sigma}^b_h \quad \text{and} \quad \mathbf{e}_{\sigma^s} \approx \mathbf{e}^*_{\sigma^s} = \boldsymbol{\sigma}^{*s}_h - \boldsymbol{\sigma}^s_h. \tag{7.2}$$

The true error may be expressed using the above notation as,

$$\|\mathbf{e}\|_{E(\Omega)} = \|\mathbf{u} - \mathbf{u}_h\|_{E(\Omega)} = \left(\int_\Omega \left(\mathbf{e}^b_\sigma\right)^T \left(\mathbf{C}^b\right)^{-1} \left(\mathbf{e}^b_\sigma\right)\, d\mathbf{x} + \int_\Omega \left(\mathbf{e}^s_\sigma\right)^T \left(\mathbf{C}^s\right)^{-1} \left(\mathbf{e}^s_\sigma\right)\, d\mathbf{x}\right)^{\frac{1}{2}}.$$

Consequently, using the approximations of Equation (7.2) the approximation of the error may be expressed as,

$$\|\mathbf{e}\|_{E(\Omega)} \approx \left(\int_\Omega \left(\mathbf{e}^*_{\sigma^b}\right)^T \left(\mathbf{C}^b\right)^{-1} \left(\mathbf{e}^*_{\sigma^b}\right) d\mathbf{x} + \int_\Omega \left(\mathbf{e}^*_{\sigma^s}\right)^T \left(\mathbf{C}^s\right)^{-1} \left(\mathbf{e}^*_{\sigma^s}\right) d\mathbf{x}\right)^{\frac{1}{2}}, \tag{7.3}$$

which we term the ZZ-P error estimator. The aforementioned recovery procedure to be employed above is that described by Zienkiewicz and Zhu in [14]. For each node a suitable patch of elements is selected which surround the node. Samples are made of the surrounding gradients at optimal (superconvergent) locations on the patch and a least squares fit to these values is then found. In the context of quadrilateral or square elements such optimal points are located at the element centroid (see Barlow, [2]). By evaluating the least squares fitted polynomial at the required node the recovered value is obtained as described in further detail in [14].

VIII. NUMERICAL EXPERIMENTS

In this section we compute finite element solutions to two test problems for which the exact solutions are known. In both cases results will be given for the JH-P estimator described in Section (V.) and for the error estimator ZZ-P estimator described in Section (VII.).

A. Bubble Problem

In this test problem we shall assume that all five displacement components as detailed in Section (II.) have the form of a bubble,

$$\zeta(\mathbf{x}) = x_1 x_2 (1 - x_1)(1 - x_2),$$

where $\mathbf{x} \equiv (x_1, x_2)^T \in \Omega$. By substituting into the equilibrium equations it is possible to compute the required load to be used in the finite element model. The plate taken will be square in shape with midplane $\Omega \equiv (0,1) \times (0,1)$ and boundary conditions $\mathbf{u}(\mathbf{x}) = \mathbf{0}$ for $\mathbf{x} \in \partial\Omega$. Material properties for the plate will be taken to be $E = 1$ and $\nu = 1/4$ in a plane stress setting which yields $\lambda = 4/15$ and $\mu = 2/5$. Setting thickness $t = 1/10$, and using Mathematica, [12], we calculate that,

$$\|\mathbf{u}\|_{E(\Omega)} \approx 6.38497465 \times 10^{-2} \quad \text{and} \quad \|\mathbf{u}\|_{L_2(\Omega)} \approx 7.45355992 \times 10^{-2}. \tag{8.1}$$

Estimator Results and Discussion Successive uniform mesh refinement of quadrilateral element meshes yields the results presented in Table (II). In this table M indicates the number of elements in the mesh, and the norms are calculated by quadrature.

TABLE II. Uniform refinement of square element uniform meshes in plate bubble problem.

h	M	$\|\mathbf{u}\|_{E(\Omega)}$	$\|\mathbf{u}_h\|_{E(\Omega)}$	$\|\mathbf{u}_h\|_{L_2(\Omega)}$	$\|\mathbf{u} - \mathbf{u}_h\|_{E(\Omega)}$
1/2	5	6.351031(−2)	5.972033(−2)	9.346701(−2)	3.360615(−2)
1/4	45	6.382858(−2)	6.264881(−2)	7.706931(−2)	1.601630(−2)
1/8	245	6.384842(−2)	6.354292(−2)	7.499261(−2)	7.928500(−3)
1/16	1125	6.384966(−2)	6.377272(−2)	7.464045(−2)	3.956547(−3)
1/32	4805	6.384974(−2)	6.383047(−2)	7.456125(−2)	1.977384(−3)
1/64	19845	6.384975(−2)	6.384493(−2)	7.454198(−2)	9.885832(−4)
1/128	80625	6.384975(−2)	6.384854(−2)	7.453719(−2)	4.942781(−4)

It can be seen from the table that the expected order of convergence is obtained for the finite element error measured in the energy norm. In addition, the computed norm values $\|\mathbf{u}_h\|_{E(\Omega)}$ and $\|\mathbf{u}_h\|_{L_2(\Omega)}$ tend to their exact values, given in (8.1), and the computed $\|\mathbf{u}\|_{E(\Omega)}$ quantity tends to the exact value. The interpolation error constants for the current set of plate data are computed to be, $C^i_{1,k} = 94.049218$ and $C^i_{2,k} = 183.711731$ (of course, six decimal places is not required in practice). Estimator performance for the set of successively refined uniform meshes can be seen in Table (III).

TABLE III. Error estimates on uniform meshes of square elements for the bubble problem.

h	ZZ-P	θ	JH-P	θ
1/2	4.207608(−2)	1.252035	6.618270	196.936289
1/4	1.693241(−2)	1.057199	3.556231	222.038246
1/8	8.068344(−3)	1.017638	1.837793	231.795810
1/16	3.977229(−3)	1.005227	9.338680(−1)	236.031038
1/32	1.980224(−3)	1.001436	4.707292(−1)	238.056558
1/64	9.889560(−4)	1.000377	2.363236(−1)	239.052839
1/128	4.943259(−4)	1.000097	1.184031(−1)	239.547534

It is clear that the ZZ-P estimator performs well by displaying the expected order of convergence and portraying asymptotically exact behaviour. First impressions of the JH-P estimator though are slightly alarming due to the large effectivity index. It is clear, however, that the JH-P estimator also converges at the expected rate. In addition, the effectivity index values do not seem to be growing in an unbounded manner and instead seem to be tending towards a value of approximately 240.

Figure (1) shows the computed order of convergence (o.o.c.) for meshes $h = 1/4$ to $1/128$ starting from initial mesh $h = 1/2$ and plotted against $\ln(M)$ using the finite element error data from Table (II) and both the ZZ-P and JH-P estimator data from Table (III).

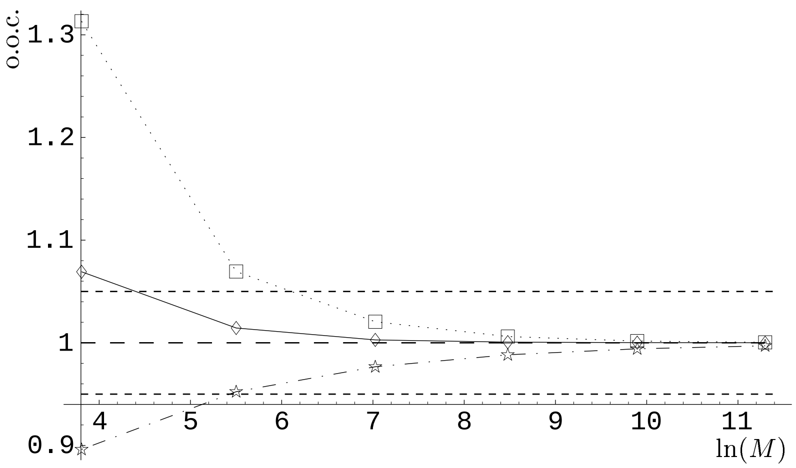

FIG. 1. Order of convergence values versus $\ln(M)$ for successively refined square element uniform meshes $h = 1/4$ to $h = 1/128$. True, ZZ-P and JH-P estimator values marked with diamond, box and star icons respectively.

The curve for the finite element error is shown as a solid line with the value at each new mesh point marked with a diamond whilst the ZZ-P and JH-P estimator curves are shown as a dotted line marked with boxes and a 'dot dash' line marked with stars respectively. Thus Figure (1) shows $O(h)$ convergence for the true error and both estimators since all three curves tend to unity as the mesh is refined. The main reason for including Figure (1), however, is in order to determine a suitable point from which a calibration constant $\mathcal{C}$ can be determined for the JH-P estimator. In this way the estimator may be scaled in order to give a global error measure so that $\theta \approx 1$. It is proposed that a suitable point at which to establish $\mathcal{C}$ will be when it is clear that $O(h)$ convergence has been attained for the first time by both the finite element error and the estimator. By denoting the order of convergence for the finite element error as α_h and that for the JH-P estimator as β_h we thus require that,

$$\max\{|\alpha_h - 1|, |\beta_h - 1|\} \leq \epsilon, \tag{8.2}$$

where ϵ is a tolerance on the deviation from unity of the two orders of convergence and which shall be taken here to be 5%. Once Equation (8.2) has been satisfied $\mathcal{C}$ can be obtained by taking the integer part of the effectivity index obtained for mesh size h. By using Equation (8.2) $O(h)$ convergence is guaranteed and the potentially troublesome early stages of the uniform refinement analyses are avoided where the order of convergence may well be much larger than unity. Figure (1) shows the 5% tolerance bounds on the theoretical order of convergence as dashed lines. It can be seen that the orders of convergence for both the finite element error and the JH-P estimator fall within these bounds for the mesh $h = 1/8$ at which point we have $\alpha_h = 1.014$ and $\beta_h = 0.952$. From Table (III) this corresponds to the integer part of the effectivity index giving $\mathcal{C} = 231$. It is accepted that the use of tolerance value ϵ is a rough rule of thumb but it is necessary to make some decision on this value in order to proceed with a JH-P estimator of an acceptable magnitude. In addition, the value of ϵ can be varied at will by the modeller depending upon what is deemed to be appropriate. By using this calibration technique, however, one can expect to obtain global error estimates from the JH-P estimator which yield an effectivity index value close to unity. Figure (2) shows the convergence curves for the finite element error measured in the energy norm and also for both the ZZ-P and calibrated JH-P error estimates upon uniform refinement.

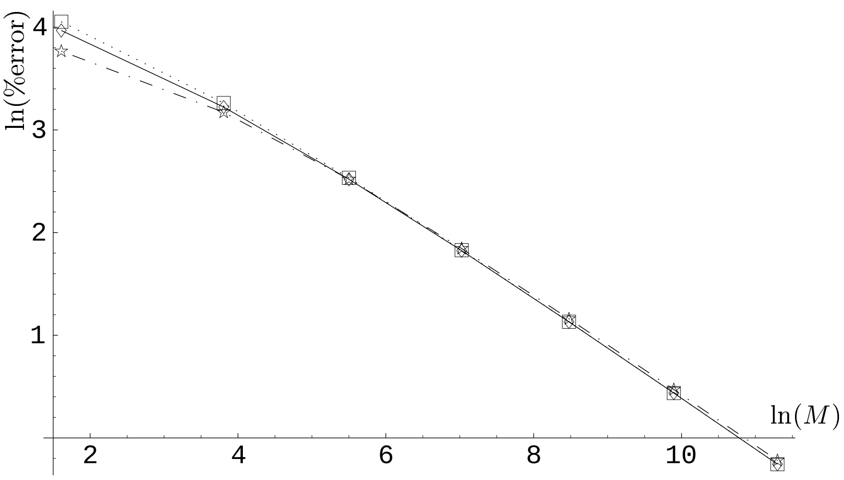

FIG. 2. Convergence curves on successively refined uniform square element meshes. True error, ZZ-P estimator and JH-P estimator marked with diamond, box and star icons respectively.

These curves are obtained as before by plotting ln(%error) against $\ln(M)$. In the same format as Figure (1) the curve corresponding to the true percentage error is shown as a solid line marked with diamonds whilst the other two percentage error curves for the ZZ-P and calibrated JH-P estimators appear as a dotted line marked with boxes and a 'dot dash' line marked with stars respectively. It can be seen that all three curves now agree closely with each other as required.

Figure (3) shows the effectivity index values for both the ZZ-P and calibrated JH-P estimators plotted against $\ln(M)$. It can be seen that $\theta \to 1$ for the ZZ-P estimator. For the case of the calibrated JH-P estimator it is clear that for the $h = 1/8$ mesh $\theta \approx 1$ whilst for coarser meshes $\theta < 1$ and for finer meshes $\theta > 1$. This is as expected due to the fact that the mesh used to obtain the calibration constant was that for $h = 1/8$ and thus the calibration constant is "tuned" to this mesh. For the coarser meshes the calibration constant is too large leading to an effectivity index of less than unity whilst for the finer meshes the calibration constant is too small leading to an overestimation in the error and an effectivity index value greater than unity. This is a result of choosing $\epsilon = 0.05$ in Equation (8.2). By choosing a smaller ϵ this will result in a calibration constant $\mathcal{C}$ being taken from a later mesh and consequently the calibrated JH-P estimator curve will cross unity at a later stage. In this way a calibration constant can be established which can force the calibrated JH-P estimator curve to cross unity at any desired point. It is, however, worth noting that it is best for an estimator to overpredict an error rather than underpredict and it is for that precise reason that a tolerance of 5% was chosen for ϵ rather than 1%.

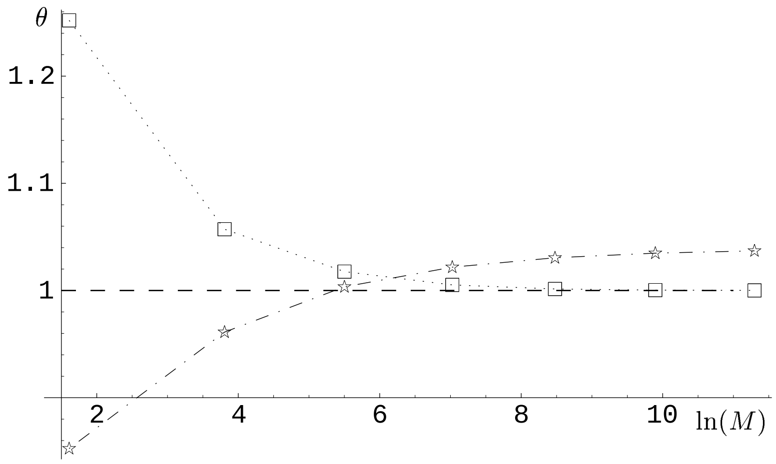

FIG. 3. Effectivity index θ versus $\ln(M)$ for ZZ-P and calibrated JH-P estimators represented by a dotted line marked with boxes and a 'dot dash' line marked with stars respectively.

Variation of Calibration Constant with Plate Thickness The previous section illustrated the proposed method for obtaining a calibration constant $\mathcal{C}$ for the JH-P estimator. It was found therein that for the current test problem a calibration constant of $\mathcal{C} = 231$ results. It is clear that by employing such a calibration constant it is possible for the calibrated JH-P estimator to attain an effectivity index close to unity as desired.

Figure (4) illustrates how the interpolation error constants C_1^i and C_2^i behave for varying plate thickness. It can be seen that for both constants C_1^i and C_2^i, whose values are marked with diamonds and boxes respectively, there is a decrease in their values as the thickness increases. This is due to the inclusion of the plate thickness in the bilinear form. For the current square plate with side dimensions or span equal to unity it is clear that a thickness value of up to two as shown in Figure (4) is excessive. Indeed the thickness of the plate should never approach the value of the plate span itself since this can no longer be considered a plate and it becomes necessary to model the body using a full three-dimensional elasticity model.

The aim of this section is to illustrate how the calibration constant $\mathcal{C}$ changes with varying plate thickness. This will be done by computing the values of $\mathcal{C}$ for a range of plate thicknesses using the method described in the previous section and Equation (8.2). For this method an accuracy of 5% is chosen on both α_h and β_h which are the orders of convergence for the finite element error and the JH-P error estimate respectively. Table

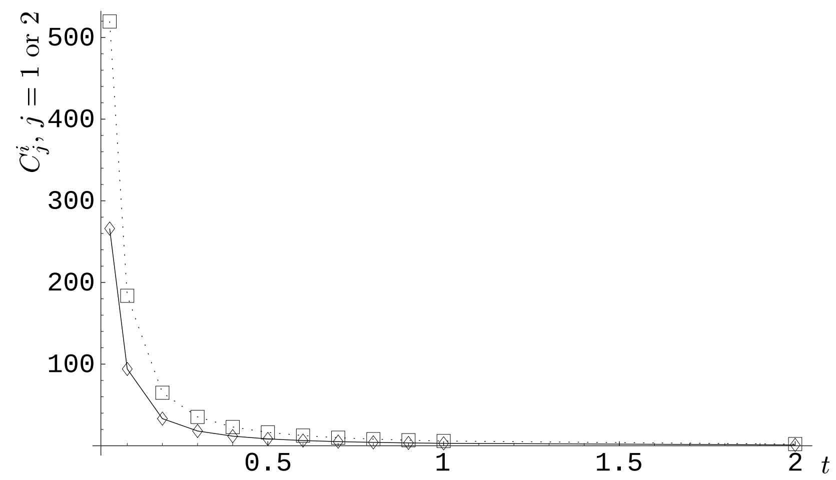

FIG. 4. Interpolation error constants C^i_1 and C^i_2 versus thickness t and denoted by a solid line marked with diamonds and dotted line marked with boxes respectively.

(IV) shows the computed values of $\mathfrak{C}$ for varying plate thickness t along with the orders of convergence from the point at which $\mathfrak{C}$ is taken.

TABLE IV. Variation of calibration constant $\mathfrak{C}$ with plate thickness t.

t	α_h	β_h	$\mathfrak{C}$
1/20	1.019	0.952	463
1/10	1.014	0.952	231
2/10	1.012	0.953	115
3/10	1.011	0.953	77
4/10	1.011	0.953	57
5/10	1.011	0.953	46
6/10	1.010	0.953	38
7/10	1.010	0.953	32
8/10	1.010	0.953	28
9/10	1.010	0.953	25
1	1.010	0.953	22
2	1.009	0.953	10

For each test in Table (IV) the plate material properties of $E = 1$ and $\nu = 1/4$ are retained and a sequence of uniformly refined meshes used to obtain $\mathfrak{C}$ as in the previous section. It can be seen that the orders of convergence α_h and β_h remain approximately constant for the thicknesses modelled. Furthermore it is found that these orders of convergence which are the first pair to satisfy Equation (8.2) are obtained throughout the analyses at mesh $h = 1/8$ as was the case in the previous section. As for the interpolation error constant illustration the thickness value is again taken to extremely large values. Further investigations reveal the model breakdown for larger thicknesses and consequently a full three-dimensional elasticity model should be implemented as previously noted.

B. Spike Problem

For this test problem we shall again assume that all five displacement components as detailed in Section (II.) have the form,

$$\zeta(\mathbf{x}) = \frac{1}{2}\exp\left(-\alpha\left((x_1 - x_1^c)^2 + (x_2 - x_2^c)^2\right)\right),$$

where the point (x_1^c, x_2^c) lies at the centre of the plate midplane which shall be taken as in the previous problem to be $\Omega \equiv (0,1) \times (0,1)$. When plotted in the x_3 direction with $\alpha = 200$ it can be seen that the displacement forms a 'spike' profile. As previously $\mathbf{u} = \mathbf{0}$ on the boundary $\partial\Omega$ and by substituting displacements into the equilibrium equations it is possible to again compute the required load to be used in the finite element model. Material properties for the plate are again taken to be $E = 1$ and $\nu = 1/4$ along with a plate thickness $t = 1/10$. This data yields energy and L_2-norm measure of the true solution calculated using Mathematica, [12], as,

$$\|\mathbf{u}\|_{E(\Omega)} \approx 3.76295844 \times 10^{-1} \quad \text{and} \quad \|\mathbf{u}\|_{L_2(\Omega)} \approx 9.90831824 \times 10^{-2}.$$

Table (V) shows the convergence of the finite element solution to that given above for a sequence of uniformly refined meshes each consisting of square elements of side h.

TABLE V. Uniform refinement of square element uniform meshes in plate spike problem.

d	$\|\mathbf{u}\|_{E(\Omega)}$	$\|\mathbf{u}_h\|_{E(\Omega)}$	$\|\mathbf{u}_h\|_{L_2(\Omega)}$	$\|\mathbf{u} - \mathbf{u}_h\|_{E(\Omega)}$
1/2	7.290559(−2)	6.886569(−1)	6.026146(−1)	7.400161(−1)
1/4	5.192551(−1)	5.102911(−1)	3.978068	8.435363(−1)
1/8	3.574541(−1)	7.493108(−1)	3.150287	5.473321(−1)
1/16	3.745532(−1)	3.595359(−1)	1.212588(−1)	1.526986(−1)
1/32	3.762958(−1)	3.687299(−1)	9.973897(−2)	8.187458(−2)
1/64	3.762958(−1)	3.743163(−1)	9.881559(−2)	4.139653(−2)
1/128	3.762958(−1)	3.757955(−1)	9.898783(−2)	2.075793(−2)

It can be seen from the table that once again the expected order of convergence is obtained for the finite element error measure and both the computed energy and L_2-norm quantities are close to their expected true values.

Due to the fact that the mesh used here is the same as that used for the previous problem the computed interpolation error constants are also the same as in the previous problem. Using the now familiar sequence of uniform meshes the estimator performance can be seen in Table (VI). It is interesting to see that again the ZZ-P error estimate is beginning to show asymptotic exactness whilst the JH-P estimator, although quicker to settle down and exhibit the theoretical rate of convergence, again overestimates the global error. The JH-P estimator θ value is approximately that found for the bubble problem for plates where $\theta \approx 239$. Using Equation (8.2) with $\epsilon = 0.05$ we obtain a calibration constant of $\mathcal{C} = 224$ here which compares well for the plate bubble problem value of $\mathcal{C} = 231$ considering the differences in the solutions.

IX. CONCLUSIONS

The numerical results show that the estimator derived from the work of Johnson and Hansbo, [4], and applied to plates is performing well. It has been noted, however, that

TABLE VI. Error estimates on uniform meshes of square elements for the spike problem.

d	ZZ-P	θ	JH-P	θ
1/2	4.869526(−1)	0.658030	8.740314(+1)	118.109788
1/4	4.259990(−1)	0.505016	6.972931(+1)	82.663079
1/8	6.429899(−1)	1.174771	7.758873(+1)	141.758051
1/16	2.180384(−1)	1.427901	3.315386(+1)	217.119603
1/32	9.945070(−2)	1.214671	1.798727(+1)	219.693002
1/64	4.453209(−2)	1.075744	9.311410	224.932104
1/128	2.119222(−2)	1.020922	4.698561	226.350181

in order to obtain a useful global error bound a calibration constant, $\mathcal{C}$, is required due to overestimation observed of the true error. It has been observed that the degree of overestimation can be quite large but at the same time it has been shown to remain approximately constant for different problems provided that the material and physical properties are retained across the problems. It is thought that the need for such a calibration constant is due to the magnitudes of the computed interpolation error constants which themselves depend upon the choice of material and physical properties of the problems. Another point to consider is that the JH-P estimator cannot take into account the possible quadrature error arising from employing the reduced integration. In order to make the computations reliable, however, the reduced integration tool is a necessary feature as the details for when a plate becomes classed as thin are by no means clearly defined.

Numerical results for the ZZ-P estimator show consistently good performance. For the test problems considered the effectivity index tends to unity at all times indicating the previously observed asymptotic exactness of the estimator.

In a further publication, [6], the above estimators will be modified to cater for the use of transition elements in the plate model. This in turn will allow the mesh to be adaptively refined and the estimator performances to be further investigated.

REFERENCES

1. Averill, R.C. and Reddy, J.N., 'Behaviour of plate elements based on the first-order shear deformation theory', *Engineering Computations*, **7**, pp.57-74, 1989.
2. Barlow, J., 'Optimal stress locations in finite element models', *International Journal for Numerical Methods in Engineering*, **10**, pp.243-251, 1976.
3. Datta, B.N., *Numerical Linear Algebra and Applications*, Brooks/Cole Publishing Company, U.S.A., 1995.
4. Johnson, C. and Hansbo, P., 'Adaptive finite element methods in computational mechanics', *Computer Methods in Applied Mechanics and Engineering*, **101**, pp.143-181, 1992.
5. Ludwig, M.J., *Finite Element Error Estimation and Adaptivity for Problems of Elasticity*, Ph.D. Thesis, Department of Mathematical Sciences, Brunel University, Uxbridge, England, 1998 (see `www.brunel.ac.uk/~icsrbicm/tech_rep.html#99`).
6. Ludwig, M.J., Shaw S. and Whiteman, J.R., 'Adaptive numerical solution of thick plates using first-order shear deformation theory. Part II: Adaptivity.', BICOM Technical Report 00/07 (see `www.brunel.ac.uk/~icsrbicm/tech_rep.html#00`). Submitted to Numer. Meth. Part. Diff. Eqns.

7. Mindlin, R.D., 'Influence of rotary inertia and shear on flexural motions of isotropic, elastic plates', *Journal of Applied Mechanics*, **18**, pp.31-38, 1951.
8. Ochoa, O.O. and Reddy, J.N., *Finite Element Analysis of Composite Laminates*, Kluwer Academic Publishers, Dordrecht, The Netherlands, 1992.
9. Oden, J.T., Demkowicz, L., Rachowicz, W. and Westermann, T.A., 'Toward a universal $h-p$ adaptive finite element strategy, PART 2. A posteriori error estimation', *Computer Methods in Applied Mechanics and Engineering*, **77**, pp.113-180, 1989.
10. Reddy, J.N., *Energy and Variational Methods in Applied Mechanics*, John Wiley & Sons, New York, 1984.
11. Reissner, E., 'The effect of transverse shear deformation on the bending of elastic plates', *Journal of Applied Mechanics, Trans. ASME*, **67**, A69-A77, 1945.
12. Wolfram, S., *Mathematica: A System for Doing Mathematics by Computer*, Addison-Wesley Publishing Company, Inc., 1991.
13. Zienkiewicz, O.C. and Zhu, J.Z.,'A simple error estimator and adaptive procedure for practical engineering analysis', *International Journal for Numerical Methods in Engineering*, **24**, pp.337-357, 1987.
14. Zienkiewicz, O.C. and Zhu, J.Z.,'The superconvergent patch recovery and *a posteriori* error estimates. Part 1: The recovery technique', *International Journal for Numerical Methods in Engineering*, **33**, pp.1331-1364, 1992.
15. Zienkiewicz, O.C. and Zhu, J.Z.,'The superconvergent patch recovery and *a posteriori* error estimates. Part 2: Error estimates and adaptivity', *International Journal for Numerical Methods in Engineering*, **33**, pp.1365-1382, 1992.